

Research Article

Numerical Investigation of the Effect of Bottom Shape on the Flow Field and Particle Suspension in a DTB Crystallizer

Hao Pan, Jun Li, Yang Jin, Bo Yang, and Xing Li

Department of Chemical Engineering, Sichuan University, Chengdu 610065, China

Correspondence should be addressed to Jun Li; lijun@scu.edu.cn

Received 16 December 2015; Accepted 8 February 2016

Academic Editor: Raghunath V. Chaudhari

Copyright © 2016 Hao Pan et al. This is an open access article distributed under the Creative Commons Attribution License, which permits unrestricted use, distribution, and reproduction in any medium, provided the original work is properly cited.

The influence of the bottom shape on the flow field distribution and particle suspension in a DTB crystallizer was investigated by Computational Fluid Dynamics (CFD) coupled with Two-Fluid Model (Eulerian model). Volume fractions of three sections were monitored on time, and effect on particle suspension could be obtained by analyzing the variation tendency of volume fraction. The results showed that the protruding part of a *W* type bottom could make the eddies smaller, leading to the increase of velocity in the vortex. Modulating the detailed structure of the *W* type bottom to make the bottom surface conform to the streamlines can reduce the loss of the kinetic energy of the flow fluid and obtain a larger flow velocity, which made it possible for the particles in the bottom to reach a better suspension state. Suitable shape parameters were also obtained; the concave and protruding surface diameter are 0.32 and 0.373 times of the cylindrical shell diameter, respectively. It is helpful to provide a theoretical guidance for optimization of DTB crystallizer.

1. Introduction

DTB crystallizer is a kind of crystallizer of high efficiency, which is widely used in chemical, food, and pharmaceutical industries [1]. With draft tube and baffles, hydrodynamics in the crystallizer become different with common stirred tank. After years of experiments and operations, DTB crystallizer has been proved to be of good performance. Crystals of larger size (the maximum can reach 600–1200 μm) can be produced. It has a higher production strength, while less crystals will adhere to the inner wall of the crystallizer, making it become one of the main forms of continuous crystallizers. The existence of a draft tube in a DTB crystallizer makes it benefit in requiring a much lower indenter to realize the inner circulation than that without a draft tube, and the power consumption can be reduced by 20% when the system reaches a certain suspension state [2, 3].

Obviously, hydrodynamics in a DTB crystallizer have a strong impact on crystallization process. In some extremely complex problems, hydrodynamics are hard to get by experiments. With the advances in computer technology and numerical techniques, Computational Fluid Dynamics (CFD) simulations, which are able to obtain fundamental

physical quantities with less time and cost, have been increasingly used to solve complex fluid mechanical problems [4, 5].

For DTB crystallizer, most researches about CFD simulations focus on the influences of structures (the impeller, the installation height of the draft tube, etc.) on the flow field distribution, the state of particle suspension, and power consumption [6–9]. Oldshue [6] investigated the suspension process using a stirred tank with a draft tube inside, and the results showed that two critical velocities should be concerned for the solid-liquid suspension operation to ensure that the particles would not deposit in the bottom; Sha and Palosaari [5] studied the influences of the structures, production discharge location, and mixing intensity on the continuous crystallization process. Jaworski et al. [7] compared the results between LDA measurements and CFD predictions to study the effects of size, location, and pumping direction of pitched blade turbine impellers on flow patterns; Zhong et al. [8] calculated the critical just off-bottom suspension impeller speed of solid-liquid system in a DTB crystallizer. Besides the impeller, draft tube, and installation location, the bottom shape of a DTB crystallizer is also an important factor that can affect the hydrodynamics of the fluid inside, which can influence the particle suspension

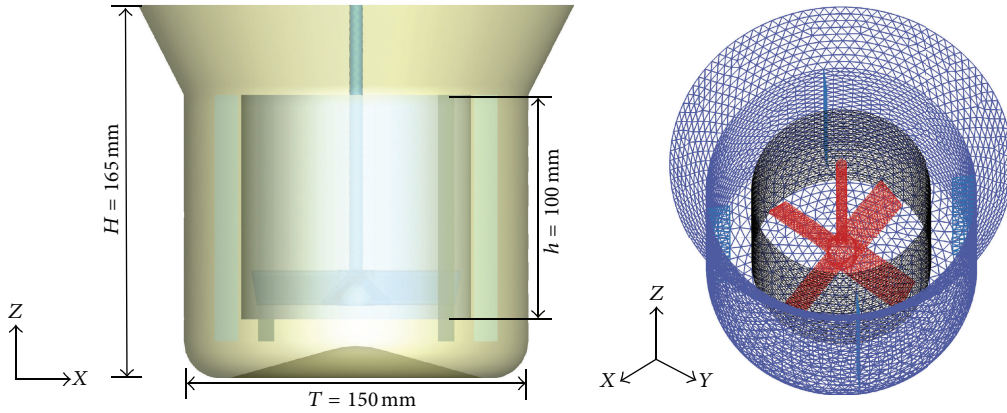


FIGURE 1: Geometry and computational grid of the investigated DTB crystallizers.

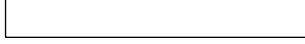

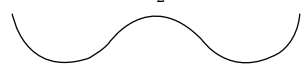

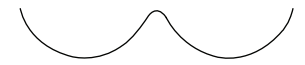
and crystallization processes [6, 9]. In the former studies, the bottom shape of the DTB crystallizer was mostly flat base or dished bottom; few researches focused on the advantages of W type bottom. The curvature of the surface of a W type bottom is more conformed to the streamlines of fluid motion generated by the combined effect of rotating impeller, baffles, and draft tube, which has advantages in particle suspension and reducing the deposition probabilities of particles at the bottom. Thus, production of larger size and more uniform particle size distribution can be available.

Suitable W type bottoms which were better for crystallization process were investigated. Five bottoms of different shapes were presented by modulating the diameters of the concave and protruding parts. Flow field distribution and particle suspension of all five DTB crystallizers with different W type bottoms were simulated by commercial software Fluent. Three representative sections were monitored on time, and graphs of volume fractions varied with flow time could be obtained. By comparing the simulation results, suitable shape parameters of W type bottom could be available, which might help to provide better hydrodynamic conditions for the crystallization process and particle suspension.

2. Geometry of the Crystallizers and Parameter Variations

Figure 1 shows the geometry of the investigated DTB crystallizers; the computational model is a proportional model to the self-made crystallizer used in the experiments. All the structure parameters are the same except the bottom shape. The total height of the crystallizer is 165 mm, the under part is made up of a 100 mm cylinder with 150 mm inner diameter and a bottom of 30 mm high, and the top part is an expanding section; the maximum diameter is 190 mm. The draft tube is 100 mm high with an inner diameter of 100 mm, and the installation height is 30 mm above the bottom. Four installed stationary baffles begin 15 mm above the bottom of the crystallizer and extend vertically over 110 mm. The diameter of the impeller is 90 mm. The computational grid applied in the CFD calculations is also showed in Figure 1. The CFD results may of course depend strongly on the employed

TABLE 1: The bottom shapes and structure parameters of the DTB crystallizers.

Number	Bottom shapes	D_1	D_2
I		—	—
II		0.320T	0.373T
III		0.373T	0.373T
IV		0.220T	0.507T
V		0.500T	0.060T

I–V are DTB crystallizers with different bottom shapes, and I–V in Figures 3, 5, 7, 8, and 9 are corresponding to those in Table 1.

mesh. In order to check grid-independency, two different meshes employing roughly 32,000 and 60,000 grid cells have been compared for a DTB crystallizer. And the results showed that there is little difference in both flow field distribution and solid particle volume fraction distribution. Therefore, the one with less grid cells is chosen for quicker simulations.

The specific bottom shapes and detailed parameters are listed in Table 1, and it shows the vertical planes of the bottoms at $Y = 0$. I is a flat bottom; II–V are W type bottoms. V is a toroidal surface bottom selected from a design manual [10], and II–IV are bottoms developed from V by some appropriate modulations. D_1 is the diameter of the concave part of the bottom and D_2 is the diameter of the protruding part of the bottom.

3. Computational Model

The solutions of the complete equations are computed by the commercial Software ANSYS-Fluent. The well known standard $k-\varepsilon$ turbulence model is adopted in the single phase simulation, and this model is based on the turbulent kinetic energy and diffusivity. Assuming that the flow field

is completely in the turbulent state, turbulent transport equations corresponding to k and ε are presented as follows:

$$\begin{aligned}\frac{\partial(\rho k)}{\partial t} + \frac{\partial(\rho k u_i)}{\partial x_i} &= \frac{\partial}{\partial x_j} \left[\left(\mu + \frac{\mu_t}{\sigma_k} \right) \frac{\partial k}{\partial x_j} \right] + G_k + G_b \\ &\quad - \rho \varepsilon - Y_M + S_k, \\ \frac{\partial(\rho \varepsilon)}{\partial t} + \frac{\partial(\rho \varepsilon u_i)}{\partial x_i} &= \frac{\partial}{\partial x_j} \left[\left(\mu + \frac{\mu_t}{\sigma_\varepsilon} \right) \frac{\partial \varepsilon}{\partial x_j} \right] \\ &\quad + C_{1\varepsilon} \frac{\varepsilon}{k} (G_k C_{3\varepsilon} G_b) - C_{2\varepsilon} \rho \frac{\varepsilon^2}{k} \\ &\quad + S_\varepsilon.\end{aligned}\quad (1)$$

According to Launder and Spalding's recommended values and experimental values, the constants in the model are equal to the numerical values below [11]; σ_k and σ_ε are Prandtl number of k and ε , respectively,

$$\begin{aligned}C_{1\varepsilon} &= 1.44, \\ C_{2\varepsilon} &= 1.92, \\ C_\mu &= 0.09, \\ \sigma_k &= 1.0, \\ \sigma_\varepsilon &= 1.3.\end{aligned}\quad (2)$$

An MRF [12] approach is applied to calculate the flow field distribution of single liquid fluid in the crystallizer. For the liquid-solid two phases flow, besides the MRF model, Eulerian model [13], which can simulate every single phase in the multiphase fluid flow, is also chosen as the total solid phase volume fraction is more than 10%. The continuity equation is formulated as

$$\frac{\partial}{\partial t} (\alpha_q \rho_q) + \nabla \cdot (\alpha_q \rho_q \vec{v}_q) = 0. \quad (3)$$

The momentum exchange between two phases is based on the momentum exchange coefficient. For liquid-solid system, the momentum exchange coefficient K_{sl} is based on the drag coefficient, and Syamlal-O'Brien model [14] is used to calculate K_{sl} when the solid phase shear stress is defined by Syamlal and O'Brien

$$\begin{aligned}K_{sl} &= \frac{3\alpha_s \alpha_l \rho_l}{4v_{r,s}^2 d_s} C_D \left(\frac{Re_s}{v_{r,s}} \right) |\vec{v}_s - \vec{v}_l|, \\ Re_s &= \frac{\rho_l d_s |\vec{v}_s - \vec{v}_l|}{\mu_l}, \\ C_D &= \left(0.63 + \frac{4.8}{\sqrt{Re_s/v_{r,s}}} \right)^2.\end{aligned}\quad (4)$$

Combining with the sedimentation velocity of the particles, the axial velocity distribution, and the impeller input

power, it is possible to compare the advantages and disadvantages of each crystallizer. Ignoring the influence between particles, the terminal velocity of the particles can be formulated simply

$$u_t = \sqrt{\frac{4 d_p (\rho_p - \rho) g}{3 C_D \rho}}. \quad (5)$$

To characterize C_D and fluid dynamics in a global manner, the modified version of the Reynolds number is used [15]

$$Re = \frac{ND_{imp}^2 \rho}{\mu}. \quad (6)$$

The calculated Reynolds number for default operating condition is approximately 108000. Therefore, a turbulence model is obviously required to describe hydrodynamics, and it can be figured out that the drag coefficient $C_D \approx 0.44$. Substituting it into (5), the terminal velocity appears:

$$u_t = 1.74 \sqrt{\frac{d_p (\rho_p - \rho) g}{\rho}}. \quad (7)$$

Shear rate is another important factor for crystallization process. In the rotation system similar to DTB crystallizer, the shear rate is a function of ε (turbulent dissipation rate) and ν (kinematic viscosity) [16, 17]:

$$\dot{\gamma} = \left(\frac{\varepsilon}{\nu} \right)^{1/2}. \quad (8)$$

The torque of the impeller can be calculated by the empirical equations [18]:

$$\begin{aligned}T_q &= \frac{\int_{\Omega} (\mu_m |\dot{\gamma}|^2) d\Omega}{2\pi N}, \\ \mu_m &= \mu \left(1 - \frac{\phi}{\phi_{max}} \right).\end{aligned}\quad (9)$$

Finally, the input power of the impeller can be calculated [19]:

$$P = 2\pi \times T_q \times N. \quad (10)$$

In all simulations, the momentum, continuity, and turbulent transport equations are numerically solved by the "SIMPLE" algorithm to predict the time-dependent variations of flow, and all simulations are unsteady. All the simulations are under the condition of 800 rpm. And the boundary and initial conditions are showed in Appendix. The results are used to predict particle volume fraction distribution and the state of suspension in DTB crystallizers with different bottom shapes.

4. Results and Discussions

4.1. Hydrodynamics. In the single liquid phase simulation, the flow time could be seen in Figure 2. The calculation

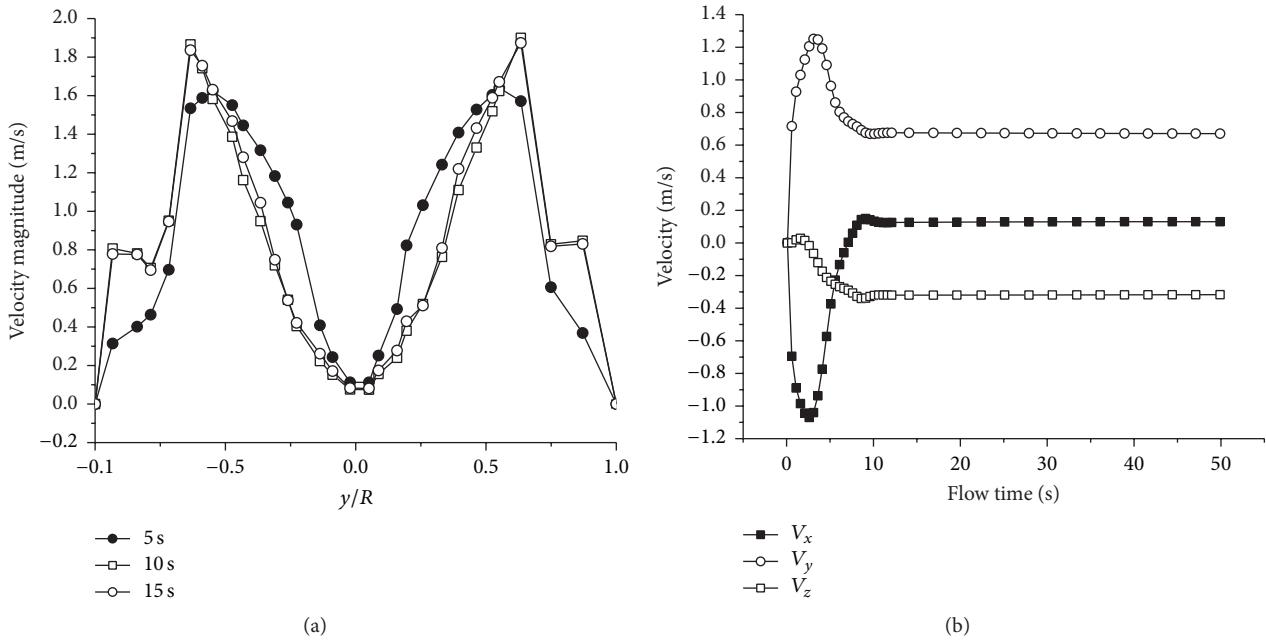


FIGURE 2: Velocity varied with time at different locations.

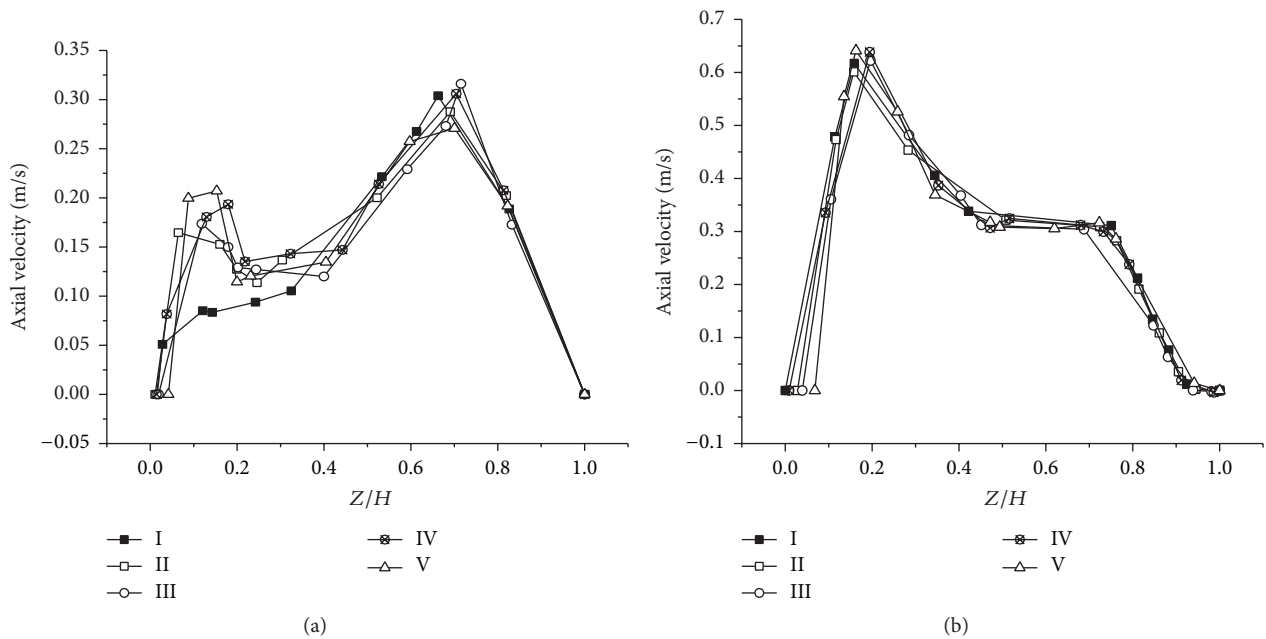


FIGURE 3: Axial velocity distributions. In (a), the radius is 60 mm and in (b) the radius is 65 mm.

time spent to reach this pattern was about 40 minutes, but it took much longer to calculate the solid-liquid two-phase simulations (about 5 hours).

Figure 2(a) showed the velocity magnitude distribution of a chosen line at different times, and we could see that the velocity distribution at 15 s was almost the same as that at 10 s. Figure 2(b) showed how the velocities (V_x , V_y , V_z) changed with flow time of one specific point. It could be obviously seen that after about 12 s, V_x , V_y , and V_z mainly remained

unchanged. Therefore, we could reach a conclusion that the flow fluid reached a steady state after about 12 s.

The axial velocity distributions at different positions in the crystallizer were showed in Figure 3. The way the flow field influences particle motions and the state of particle suspension could be reflected indirectly. Figures represented the velocities of straight lines from bottom to top between draft tube and outside wall of the crystallizer. Since a periodicity and symmetry condition along the azimuthal direction could

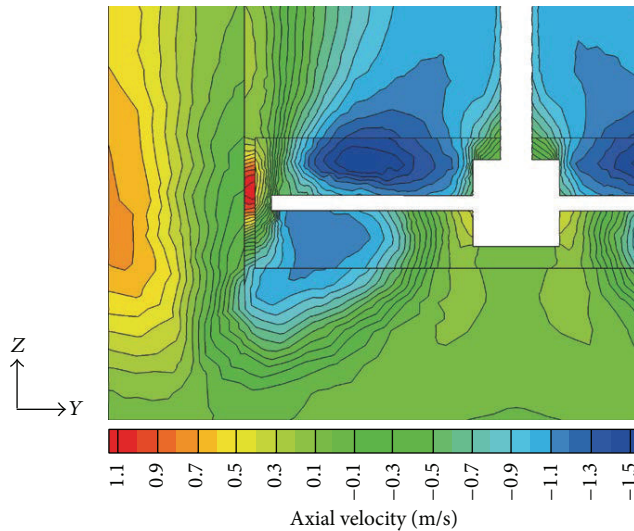


FIGURE 4: Axial velocity distribution below the draft tube in the flat bottom crystallizer.

be invoked for the flow field, it was reasonable to determine the position of the straight lines by the value of radius (r). In Figure 3 and all the following figures, I represents flat bottom and II–V represent W type bottoms.

Figure 3(a) showed the axial velocity of the line at $R = 60$ mm; the positive values meant the fluid flows upward, and vice versa. The axial velocity of I was lower than that of II–V when $Z/H < 0.2$; that is, the distance from the bottom was approximately 30 mm, which represented the region below the draft tube. In this area, the axial velocity of I was lower than 0.1 m/s, while the axial velocities in II–V were obviously larger than I and probably reached 0.2 m/s. When $Z/H > 0.2$, the variation tendency of axial velocities in I–V basically varied similarly. Nevertheless, at $R = 65$ mm, the variation tendency of axial velocities in I–V basically remained the same, and the values could exceed 0.2 m/s when Z/H was larger than 0.1. Based on (7), the terminal velocity of the particles (u_t) could be calculated to be 0.157 m/s. The absolute velocity ($u_p = u - u_t$) of the particles was directly related to the hydrodynamics of the fluid. Only $u \geq 0.157$ m/s could make it possible for the particles to move with the fluid and suspend in the crystallizer. Comparing u_t with Figure 3, it was obvious to see that, at $R = 60$ mm under the draft tube, flow velocities in II–V were larger than u_t ; particles in II–V should be more likely to reach the state of complete suspension than those in I.

Figure 4 showed the axial velocity distribution of the lower part in crystallizer I. As the legend showed, the positive value means the fluid moves upward; otherwise the fluid flows downward. It was obvious to know that just below the draft tube the axial velocities in all five cases were downward, and the axial velocities of the near crystallizer wall annulus region were all greater than 0.157 m/s. Hence, what needed to be discussed was the near draft tube annulus region. Because of the interaction between the two phases, the axial velocity would decrease when the solid particles were added under the same conditions [20]. In the near draft tube annulus region,

TABLE 2: Impact of stirring speed on input power of the impeller.

Stirring speed/rpm	Torque/N·m	Power/W·m ⁻³
800	0.1947	16.31
1000	0.4987	52.19

axial velocity was lower than 0.157 m/s; it could be seen that the axial velocity would get smaller so that the flowing fluid was unable to carry the particles. Therefore, complete suspension of particles was not achievable in this area. On the contrary, particles were more likely to deposit and accumulate in the bottom, which could affect the crystallization process and the size of ultimate production. As was discussed above about Figure 3, the axial velocities of II–V in the same region were greater than 0.157 m/s, which was benefit for the particle suspension and crystal growth. The state of suspension could be improved by increasing stirring speed, accompanying the increase of power consumption. Therefore, the performance of the flat bottom DTB crystallizer was not as good as the W type bottom crystallizers.

A comparison of the input power of the impeller with different stirring speed, which was calculated by (10), was showed in Table 2. The input power of the impeller increased as the stirring speed increases, but the rates of increase varied a lot. The input power appeared as an increase of 3.2-fold, while the stirring speed merely increased by 1.25-fold. With the increase of the stirring speed, the metastable region shrank, which made it easier to generate more fine grains. And the increase of flow-shear stress also enhanced the possibility of collisions between crystals, which resulted in the increase of the second nucleation rate [21]. Hence, due to the extra consumption of energy and bad influence on the crystallization process, flat bottom was inappropriate to use.

Figure 5 showed the streamlines in the vertical planes ($Y = 0$) of different crystallizers under the same conditions. The more intensive the streamlines were, the larger the flow velocity was. The distributions of the streamlines were roughly the same in five vertical planes. Eddies created by recirculation of the fluid existed below the impeller, in the outlet and inlet of the draft tube in all five crystallizers, but eddies were not the same size and the intensities of the streamlines differ delicately. Eddies below the impeller had the greatest influence on the particles suspension. Particles moved with the fluid and there were two main motion paths till the particles arrived at the outlet of the draft tube. First, particles moved into the annulus area and then continued to move upward. Second, particles moved into the eddies below the draft tube, spinning around or accumulating in the bottom. It was obvious to see that eddies in I and V are bigger than others, making it more probable for the particles to move according to the second way. Streamlines in these eddies were less intensive, which meant the velocities were lower and more particles would deposit relatively. On the contrary, eddies in II and III were smaller; thus more particles would move in the first way. Meanwhile streamlines in II were more intensive, which meant the velocity was higher and the aqueous carrying capacity of particles could be greater. Therefore, W type bottoms should be better than flat bottom for

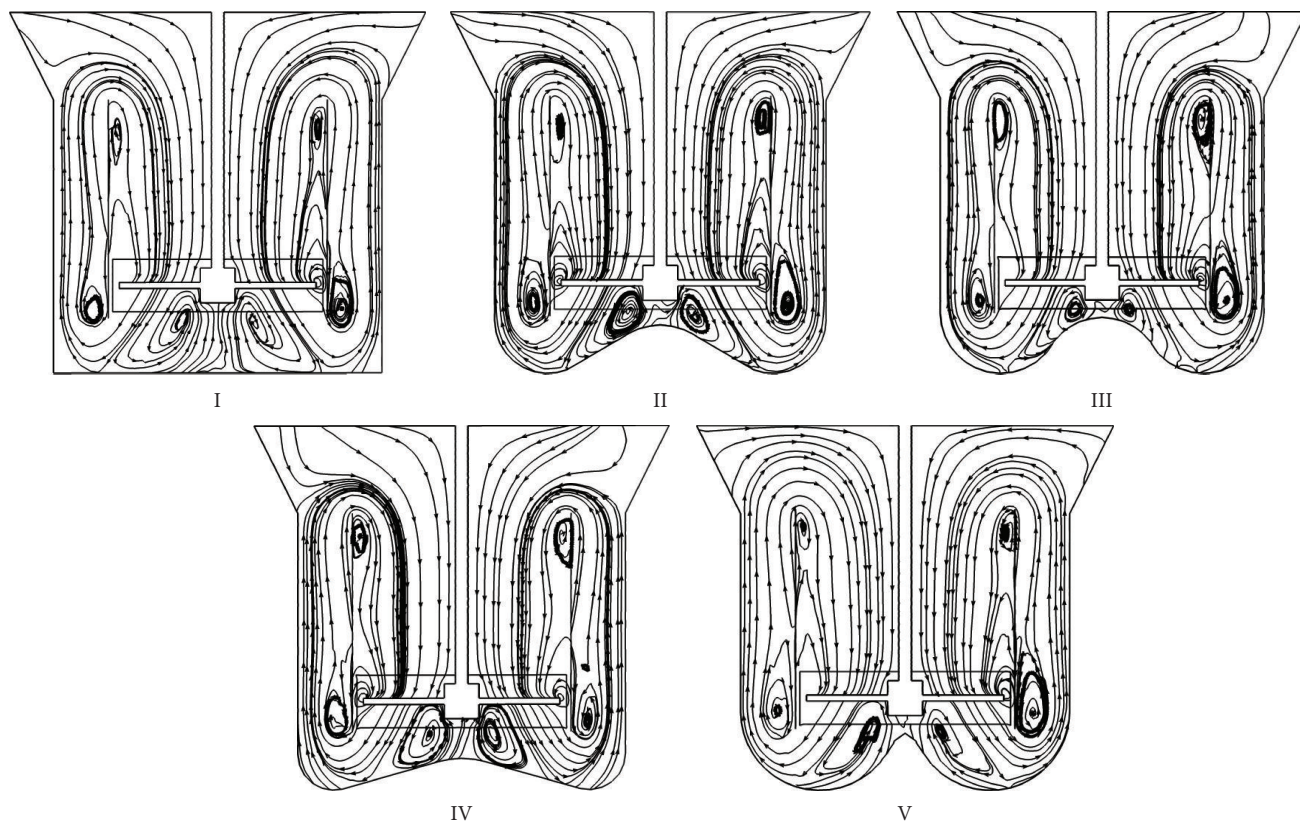


FIGURE 5: Comparison of instantaneous streamlines neglecting the velocity component perpendicular to the cutting plane (vertical plane $Y = 0$).

the crystallization process and fine distinctions in the shape parameters of the bottom could affect the hydrodynamics and make a difference in the particle suspension.

4.2. Particle Suspension. In order to elaborate the detailed differences between the different W type bottoms, further simulations were investigated. Particle size distribution of the ultimate production had a certain requirement in industry. In this work, the average size of the particles was $500 \mu\text{m}$. Therefore, monosized particles of $500 \mu\text{m}$ were chosen to investigate the state of suspension in each crystallizer with different bottom shapes. The rotating speed of impellers remained 800 rpm, and other physical property parameters of liquid phase remained the same. The total volume fraction of solid particles was 10 vol%. In order to observe the volume fraction of the particles in the bottom of the crystallizers intuitively, volume fractions of three sections were monitored on time. The three sections were showed in Figure 6. Sections A and B were transversal surfaces of the crystallizer at different heights, while section C was part of the longitudinal surface of the crystallizer at $Y = 0$.

By monitoring the volume fractions in section A and section B, we could figure out the state of suspension in the bottom of the crystallizers. The value of the volume fraction in section A reflected the amount of the particles in the bottom of the crystallizers to some extent. Because below section A, the volume fraction should be larger theoretically.

Simultaneously, the comparison between A and B showed the homogeneity of the particle distributions in whole crystallizers. The smaller the difference of values between A and B was, the more homogeneous the particles were distributed. The results were showed in Figure 7.

In order to investigate the state of suspension of the particles in the bottom, the monitoring of section C in all five DTB crystallizers were showed in Figure 8 as a further illustration. Because of the periodicity and symmetry of the fluid flow in the DTB crystallizer, the equilibrium value of the volume fraction in section C could account for the particle suspension more accurately. More particles deposited in the bottom when the value of volume fraction got larger, and the flow-ability of the fluid got worse; more particles accumulated in the bottom, which resulted in the nonuniform distribution of the particles, and the ultimate size of productions was uneven.

As the results showed in Figures 7 and 8, it was obvious to figure out that, in all the five DTB crystallizers with different bottom shapes, the volume fractions of the solid particles arrived at an equilibrium state after stirring for 100 s, which meant that, under the condition of 800 rpm, the influence of the bottom shape on the mixing efficiency was tiny enough to neglect. Although the time to attain an equilibrium remained the same, the numerical values of volume fraction in the state of equilibrium in section A, section B, and section C differed a lot.

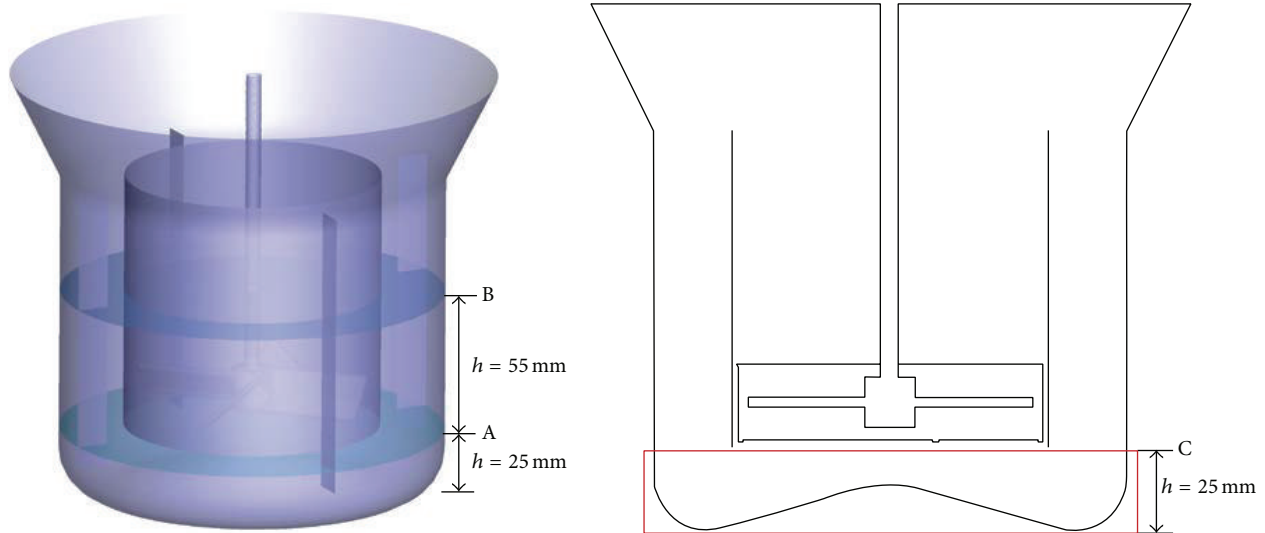


FIGURE 6: The chosen sections to monitor the volume fractions.

As expected, it was observed that volume fractions of section B were larger than those of section A in II and III when the mixing of the particles reached an equilibrium state, while in I and IV the volume fractions of section B were smaller than those of section A, which meant more particles accumulated in the bottom part of the crystallizers. In V, the two values were equaled. In II and III, the volume fractions of section B were larger than those of section A, which meant less particles deposited in the bottom but more particles suspended in the middle part of the crystallizers. It was better to see that the volume fraction value in section A remained smaller than that in section B, which meant more crystals suspended in the middle part of the crystallizer. And in case V, the volume fraction of section A equaled the value in section B; the particle distribution was more uniform but the volume fraction value was a little larger than that of II and III. Therefore we could see that the suspension state in case V was not the best one. As discussed above, in II and III, eddies under the rotating impeller were smaller than the others; thus less particles moved according to the second way and the volume fraction of section A got smaller. In I, IV, and V, eddies got much bigger and the velocities inside the vortices got lower; the ability for the flow fluid to carry the particles moving with it became weaker, resulting in the accumulation of particles in the bottom.

The consequences of the monitoring of the volume fractions of particles in section A and section B in liquid-solid two-phase simulations were conformed to the results in the investigations of hydrodynamics in single phase simulation. It had been surprising to see the great differences of hydrodynamics and deposition probabilities caused by the different bottom shapes. To investigate this issue further, it was essential to continue to monitor the volume fraction of the particles in section C to verify the suspension property between II and III.

Figure 8 shows the volume fractions varied with flow time in section C in all the crystallizers with different bottoms. It

was more intuitive to see the amount of particles accumulate in the bottom part of the whole crystallizer. The volume fractions in I and V were larger than the others and it was corresponding to the results of single phase simulation. The volume fractions of III and IV were smaller than those of I and V. Although the numerical values of III and IV were basically the same, the volume fraction of section A in III was smaller than IV, which means the total amount of particles in the bottom of III was larger than IV. Therefore, the bottom shape of III was not good enough to improve the hydrodynamics and promote the suspension property. It was obvious to see that the volume fraction of II was much smaller than the others, which meant the influence of the bottom shape on the hydrodynamics was positive and it was benefit to the suspension of the particles. More particles in II moved in the first way mentioned above, which was good to the particle suspension and has advantages in the crystallization process. All the conclusions are conformed to the results in Section 4.1. The reason why bottom shape had a great influence was that W type bottoms with different structures and parameters affected the fluid flow distribution. The protruding part of the bottom broke the eddies, making them become smaller, so that less particles would move into the eddies in the bottom part of the crystallizers and just span in the bottom, which prevented the solid particles gathering and aggregating. Therefore, it was important to design an appropriate W type bottom.

As mentioned above, we have discussed the state of particle suspension in all five DTB crystallizers with the total solid particles which amount to 10 vol%. The results show that II is better than the others in the suspension property under this condition. In order to make further verification that the hydrodynamics of II is superior to the others in particle suspension, volume fractions of section C vary with flow time under the conditions of the solid particles which amount to 15 vol% and 20 vol% depicted in Figure 9.

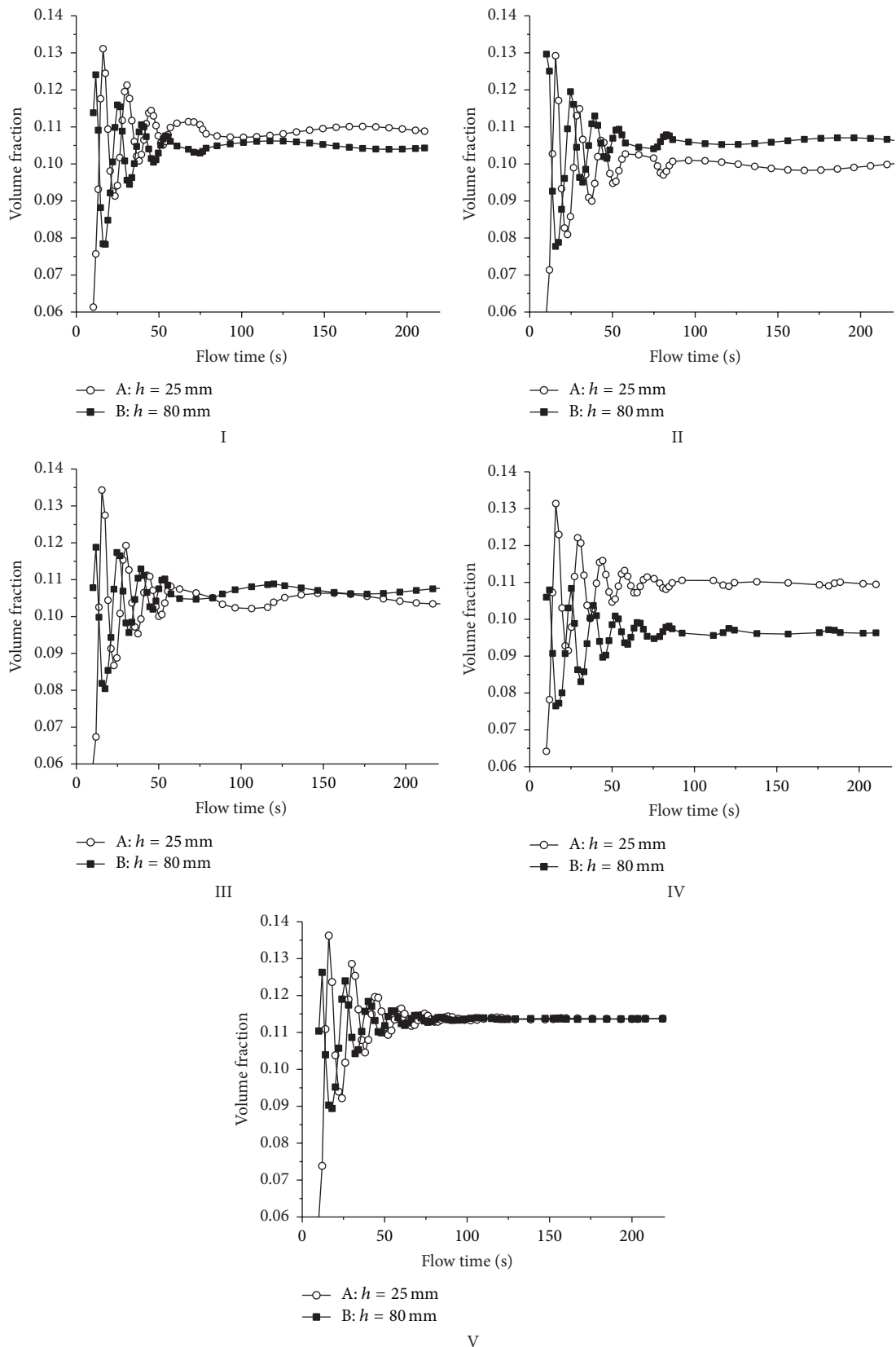


FIGURE 7: Volume fractions vary with flow time in sections A and B.

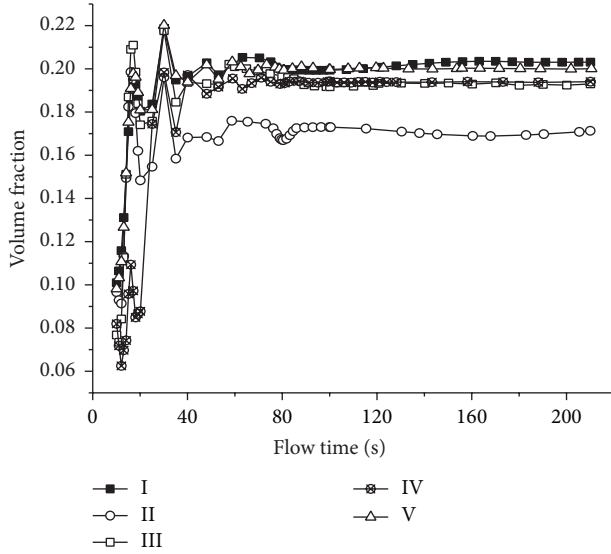


FIGURE 8: Volume fractions vary with flow time in section C.

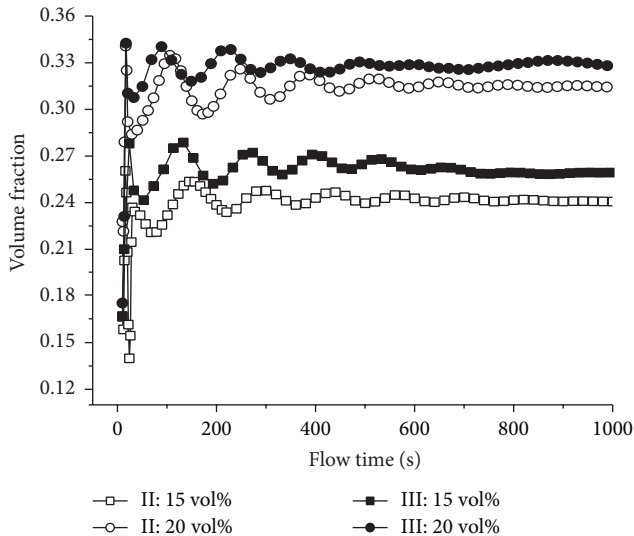


FIGURE 9: Volume fractions vary with flow time in section C with different initial total particle volume fractions.

The above statements are confirmed that the suspension property of III is second to II. Therefore, the state of particle suspension is only compared between II and III. In Figure 9, it is obvious to see that when the initial particle volume fraction increases to 15% or 20%, the total flow time for the volume fractions in section C arriving at an equilibrium state gets longer than that of 10 vol% of particles. Whether the initial particles amount to 15 vol% or 20 vol%, the volume fraction of II is always smaller than that of III, which means less particles in II deposit in the bottom region. Therefore, more particles move upward with the fluid; the hydrodynamics in II make the particles reach a better suspension state, which prevents the accumulation and agglomeration of the particles, and more uniformly distributed production is available. Nevertheless, with the initial particle volume fraction increasing, the

TABLE 3: Unevenness of the particle distribution.

Volume fraction	II unevenness	III unevenness
10%	59.04%	67.33%
15%	44.18%	47.76%
20%	29.76%	34.24%

TABLE 4: Input power of the impeller with different amount of particles.

Volume fraction	II		III	
	Torque/N·m	Power/W·m ⁻³	Torque/N·m	Power/W·m ⁻³
10%	0.1852	15.51	0.1857	15.55
15%	0.1988	16.65	0.1997	16.72
20%	0.2122	17.77	0.2139	17.91

difference between II and III gets narrow, and it is known that the advantages of hydrodynamics generated by bottom shape like II could only be reflected in a low particle content. As the amount of particles gets too large, the advantages of the hydrodynamics of flow fluid made by the special bottom shape are not enough to offset the impact created by the interaction of the two phases, which means it is necessary to remove the particles from the crystallizer in time to make the total particle amount maintain a good suspension property.

The analysis above majorly focuses on the distribution of the solid particles in the bottom part of the DTB crystallizer. The emphasis of the study is to investigate the way the shape of bottom affects the hydrodynamics and further influences the particle suspension. Therefore, it helps to prevent the excessive accumulation of the particles, which is helpful to avoid the bad influence on the crystallization process and equipment operation. In order to investigate the suspension uniformity in the whole crystallizer, the concept of unevenness is introduced, and the unevenness is defined as follows:

$$M = \left[\frac{1}{n} \sum_{i=1}^n \left(\frac{C_i - \bar{C}}{\bar{C}} \right)^2 \right]^{0.5} \quad (11)$$

The unevenness of the particle distribution of II and III under different conditions is showed in Table 3.

From Table 3, it is apparent to see that the evenness of the particle distribution of II is always smaller than that of III, which means the particles are better distributed in II.

Table 4 shows the input power of the impeller with different amount of particles, and as expected, power consumption of II is always less than that of III, which further prove that II is better than the others, not only in the good performance in particle suspension, but also in the lower cost of energy.

5. Conclusion

Numerical simulations are conducted to investigate the effect of bottom shape on the hydrodynamics and particle suspension. It is found that the bottom shape has significant

TABLE 5: Boundary and initial conditions of the simulations.

Crystallizer parts	Boundary conditions
Baffle	Wall motion: stationary wall Shear condition: no slip
Impeller	Wall motion: moving wall
Shaft	Wall motion: moving wall
Draft tube	Wall motion: stationary wall
Walls of crystallizer	Wall motion: stationary wall Shear condition: no slip
Rotating region	800 rpm
Initial particle volume fraction	10 vol% of the whole crystallizer

influence on the flow field distribution. Under the effect of the rotating impeller agitation, vortices can be created by the fluid flows in a restricted space as a DTB crystallizer, and the vortices then become an important factor affecting the particle suspension. The W type bottom can counteract the impact brought by the eddies to some extent. The presence of the protruding part can destroy the main eddies under the draft tube, making them become smaller than before. With the vortices being smaller, less particles will move into the vortices when they arrived at the outlet of the draft tube; more particles will move into the annulus region and continue moving upward. Meanwhile, the smooth surface of the concave part of the bottom is much more conformed to the streamlines, which decrease the energy consumption of the fluid flow. This is how the bottom shape affect the hydrodynamics and consequently affect particle suspension and crystallization process. Comparing the simulation results of crystallizers with different bottoms, it can be known that different W type bottoms have different effects on hydrodynamics; it is important to find suitable shape parameters of the bottom for suspension advantaged hydrodynamics and less energy consumption. In general, the CFD simulation is capable of providing theoretical guidance for design and optimization of DTB crystallizer.

Appendix

See Table 5.

Nomenclature

d_p :	Particle diameter, mm
H :	Crystallizer height, mm
h :	Draft tube length, mm
T :	Cylindrical shell diameter, mm
D :	Draft tube diameter, mm
D_1 :	Concave surface diameter of the bottom, mm
D_2 :	Protruding surface diameter of the bottom, mm
D_{imp} :	Impeller diameter, mm
N :	Impeller rotating speed, rpm

k :	Turbulent kinetic energy, $m^2 \cdot s^{-2}$
K_{sl} :	Momentum exchange coefficient, s^{-1}
C_D :	Drag coefficient
P :	Power, $W \cdot m^{-3}$
T_q :	Impeller torque, $N \cdot m$
u :	Fluid flow velocity, $m \cdot s^{-1}$
u_p :	Particle velocity, $m \cdot s^{-1}$
u_t :	Terminal velocity, $m \cdot s^{-1}$
n :	Number of sampling locations
M :	Unevenness
C_i :	Particle volume fraction
\bar{C} :	Weighted average particle volume fraction
t :	Time, s
$v_{r,s}$:	Particle's terminal velocity, $m \cdot s^{-1}$
$C_{1\varepsilon}, C_{2\varepsilon}, C_\mu$:	Standard coefficients for k - ε turbulence model.

Greek Letters

ρ :	Density, $kg \cdot m^{-3}$
μ :	Viscosity, Pa·s
ε :	Turbulent dissipation rate, $m^2 \cdot s^{-3}$
Φ :	Particle concentration
Φ_{max} :	Maximum particle concentration
ν :	Kinematic viscosity, $m^2 \cdot s^{-1}$
$\dot{\gamma}$:	Shear rate, s^{-1}
α_s :	Solid phase volume fraction
α_l :	Liquid phase volume fraction
$\sigma_k, \sigma_\varepsilon$:	Standard coefficients for k - ε turbulence model.

Dimensionless Number

Re: Reynolds number, $Re = \rho N d^2 / \mu$.

Subscripts

s :	Solid phase
l :	Liquid phase
p :	Particles.

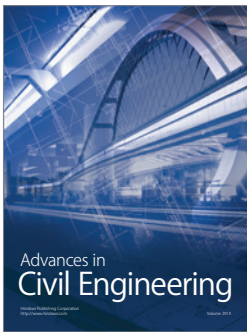
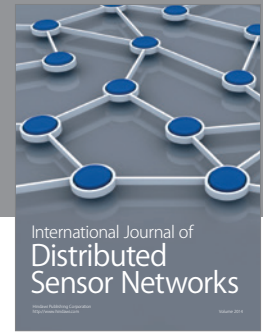
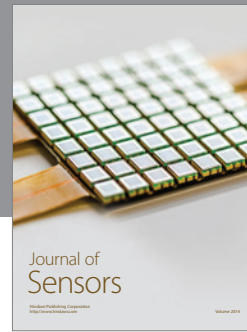
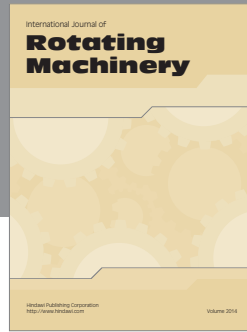
Conflict of Interests

The authors declare that there is no conflict of interests regarding the publication of this paper.

References

- [1] Y. C. Huang, J. Tang, and R. Q. Xie, "Applications of computational fluid dynamics in chemical engineering," *Modern Chemical Industry*, vol. 27, no. 5, pp. 65–68, 2007.
- [2] S. J. Shiue and C. W. Wong, "Studies on homogenization efficiency of various agitators in liquid blending," *The Canadian Journal of Chemical Engineering*, vol. 62, no. 5, pp. 602–609, 1984.
- [3] F. J. Wang, *Computer Fluid Dynamics Analysis—Principles and Applications of CFD*, Tsinghua University Press, Beijing, China, 2004.

- [4] C. R. Liu, A. D. Huhe, and W. J. Ma, "Numerical and experimental investigation of flow over a semicircular weir," *Acta Mechanica Sinica*, vol. 18, no. 6, pp. 594–602, 2002.
- [5] Z. Sha and S. Palosaari, "Modeling and simulation of crystal size distribution in imperfectly mixed suspension crystallization," *Journal of Chemical Engineering of Japan*, vol. 35, no. 11, pp. 1188–1195, 2002.
- [6] J. Y. Oldshue, *Fluid Mixing Technology*, edited by: Y. C. Huang, M. L. Ling Trans, Chemical Industrial Press, Beijing, China, 1991.
- [7] Z. Jaworski, K. N. Dyster, and A. W. Nienow, "The effect of size, location and pumping direction of pitched blade turbine impellers on flow patterns: LDA measurements and CFD predictions," *Chemical Engineering Research and Design*, vol. 79, no. 8, pp. 887–894, 2001.
- [8] L. Zhong, X. B. Huang, and Z. G. Jia, "CFD modeling of solids just suspended impeller speed in stirred tanks," *Journal of Beijing University of Chemical Engineering*, vol. 30, no. 6, pp. 18–22, 2003.
- [9] D. H. Xie, "DTB type crystallizer," *Chemical Engineering & Machinery*, vol. 21, no. 1, pp. 55–57, 1994.
- [10] Z. P. Chen, X. W. Zhang, and X. H. Lin, *Stirring and Mixing Equipment Design Manual*, Chemical Industry Press, 1st edition, 2004.
- [11] B. E. Launder and D. B. Spalding, *Lectures in Mathematical Models of Turbulence*, Academic Press, London, UK, 1972.
- [12] J. Y. Luo, R. I. Issa, and A. D. Gosman, "Prediction of impeller-induced flows in mixing vessels using multiple frames of reference," *Icheme Symposium Series*, vol. 136, pp. 549–556, 1994.
- [13] D. A. Drew and R. T. Lahey, *In Particulate Two-Phase Flow*, Butterworth Heinemann, Boston, Mass, USA, 1993.
- [14] M. Syamlal and T. J. O'Brien, "Computer simulation of bubbles in a fluidized bed," *AIChE Symposium Series*, vol. 85, no. 270, pp. 22–31, 1989.
- [15] B. Ashraf Ali, G. Janiga, E. Temmel, A. Seidel-Morgenstern, and D. Thévenin, "Numerical analysis of hydrodynamics and crystal motion in a batch crystallizer," *Journal of Crystal Growth*, vol. 372, pp. 219–229, 2013.
- [16] S. A. Altobelli, R. C. Givler, and E. Fukushima, "Velocity and concentration measurements of suspensions by nuclear magnetic resonance imaging," *Journal of Rheology*, vol. 35, no. 5, pp. 721–734, 1991.
- [17] F. E. Kruis and K. A. Kusters, "The collision rate of particles in turbulent flow," *Chemical Engineering Communications*, vol. 158, pp. 201–230, 1997.
- [18] L. Fradette, P. A. Tanguy, F. Bertrand, F. Thibault, J.-B. Ritz, and E. Giraud, "CFD phenomenological model of solid-liquid mixing in stirred vessels," *Computers and Chemical Engineering*, vol. 31, no. 4, pp. 334–345, 2007.
- [19] F. A. Holland and F. S. Chapman, *Liquid Mixing and Processing in Stirred Tank*, Reinhold Publishing Corporation, New York, NY, USA, 1966.
- [20] Y. Y. Bao, X. B. Huang, L. T. Shi, and Y. C. Wang, "The influence of solid particles on fluid velocity in a stirred tank," *Chemical Engineering (China)*, vol. 30, no. 5, pp. 29–33, 2002.
- [21] A. Van Hook, *Crystallization Theory and Practice*, Chapman & Hall, London, UK, 1961.



Hindawi

Submit your manuscripts at
<http://www.hindawi.com>

